Radiative Carrier Lifetime in $Ge_{1-x}Sn_x$ Mid-Infrared Emitters

Gérard Daligou,[1] Anis Attiaoui,[1] Simone Assali,[1] Patrick Del Vecchio,[1] and Oussama Moutanabbir[1,*]

[1]*Department of Engineering Physics, École Polytechnique de Montréal, C.P. 6079, Succ. Centre-Ville, Montréal, Québec, Canada H3C 3A7*

$Ge_{1-x}Sn_x$ semiconductors hold the premise for large-scale, monolithic mid-infrared photonics and optoelectronics. However, despite the successful demonstration of several $Ge_{1-x}Sn_x$-based photodetectors and emitters, key fundamental properties of this material system are yet to be fully explored and understood. In particular, little is known about the role of the material properties in controlling the recombination mechanisms and their consequences on the carrier lifetime. Evaluating the latter is in fact fraught with large uncertainties that are exacerbated by the difficulty to investigate narrow bandgap semiconductors. To alleviate these limitations, herein we demonstrate that the radiative carrier lifetime can be obtained from straightforward excitation power- and temperature-dependent photoluminescence measurements. To this end, a theoretical framework is introduced to simulate the measured spectra by combining the band structure calculations from the *k.p* theory and the envelope function approximation (EFA) to estimate the absorption and spontaneous emission. The model computes explicitly the momentum matrix element to estimate the strength of the optical transitions in single bulk materials, unlike the joint density of states (JDOS) model which assumes a constant matrix element. Based on this model, the temperature-dependent emission from $Ge_{0.83}Sn_{0.17}$ samples at a biaxial compressive strain of -1.3% was investigated. The simulated spectra reproduce accurately the measured data thereby enabling the evaluation of the steady-state radiative carrier lifetimes, which are found in the 3-22 ns range for temperatures between 10 and 300 K at an excitation power of $0.9\,kW/cm^2$. For a lower power of $0.07\,kW/cm^2$, the obtained lifetime has a value of 1.9 ns at 4 K. The demonstrated approach yielding the radiative lifetime from simple emission spectra will provide valuable inputs to improve the design and modeling of $Ge_{1-x}Sn_x$-based devices.

I. INTRODUCTION

$Ge_{1-x}Sn_x$ alloys constitute an emerging class of group IV semiconductors providing a tunable narrow bandgap, which has been highly attractive to implement scalable, silicon-compatible mid-infrared photonic and optoelectronic devices [1]. This potential becomes increasingly significant with the recent progress in nonequilibrium growth processes enabling high Sn content $Ge_{1-x}Sn_x$ layers and heterostructures leading to the demonstration of a variety of monolithic mid-infrared emitters and detectors [2–18]. Notwithstanding the recent developments in device engineering, the impact of structural characteristics on the basic behavior of charge carriers is yet to be fully understood. This includes the role of Sn content, lattice strain, and growth defects in shaping the nature and magnitude of the recombination mechanisms and their consequences on the carrier lifetime. Particularly, investigating the latter remains a daunting task due to the lack of methods and tools that can be applied to probe charge carriers in narrow bandgap materials. For instance, time-resolved photoluminescence (PL) can hardly be applied to investigate materials at emission wavelengths in the mid-infrared range as high-speed detectors covering this range are not broadly available. Thus, the very few reported time-resolved studies concern $Ge_{1-x}Sn_x$ emitting below 2.3 µm corresponding to a relatively low Sn content and/or highly compressively strained materials [19–21].

In an attempt to circumvent the aforementioned limitations, a recent study employed time-resolved PL with a nonlinear crystal allowing the up-conversion of photons emitted to a shorter wavelength that can be detected by a conventional silicon-based avalanche photodiode [19]. An effective carrier lifetime of 217 ps at 20 K was estimated for $Ge_{0.875}Sn_{0.125}$ with -0.55% strain using this method [19]. Additionally, by investigating spin-dependent optical transitions leveraging the Hanle effect under steady-state excitation, systematic studies combining modeling and magneto-PL analysis of pseudomorphic layers at a Sn content below 10% reported a radiative lifetime in the 0.5-2.5 ns range at 10 K [20]. However, significantly higher carrier lifetimes reaching 450 ns were recently reported for $Ge_{1-x}Sn_x$ ($x < 0.06$) grown on InAlAs buffer layers as measured by contactless microwave photoconductive decay [21]. This scarcity of studies on carrier dynamics in narrow bandgap $Ge_{1-x}Sn_x$ semiconductors limits the understanding of their fundamental behavior and burdens the development of accurate and predictive models for $Ge_{1-x}Sn_x$-based mid-infrared optoelectronic devices.

In this work, we demonstrate that straightforward PL analyses along with the proper theoretical framework are sufficient to alleviate these challenges and extract the radiative carrier lifetime in $Ge_{1-x}Sn_x$ mid-infrared emitters and evaluate its evolution as a function of temperature. The approach relies on the simulation of the experimental PL spectra by combining the band structure calculations using the *k.p* formalism together with the EFA to estimate the absorption and spontaneous emission spectra.

* oussama.moutanabbir@polymtl.ca

arXiv:2302.02467v2 [physics.app-ph] 9 Feb 2023

Unlike the JDOS model, in which the momentum matrix element is considered constant, the oscillator strengths are explicitly computed in this model.

In the following sections, the model is described followed by the experimental demonstration using as-grown $Ge_{0.83}Sn_{0.17}$ layers, emitting at wavelengths above 3 µm.

II. THEORETICAL FRAMEWORK

The PL spectrum intensity is usually determined using the direct interband emission theory and the spontaneous emission spectrum [22]. Indeed, by considering a slab of homogeneously excited material, Lasher and Stern [23] and Würfel [24] expressed the *external* flux of spontaneous radiative emission in terms of the spectral absorptivity under non-equilibrium conditions in terms of the quasi-Fermi level splitting, $\Delta\mu = \mu_e - \mu_h$. The resulting "Lasher-Stern-Würfel" (LSW) equation is

$$I_{\mathrm{PL}}(E) = \frac{2\pi}{\hbar^3 c^2} \frac{E^2 a(E)}{\exp\left(\frac{E-\Delta\mu}{k_{\mathrm{B}}T}\right) - 1} = \frac{a(E)}{\alpha(E)} \cdot \frac{r^{\mathrm{sp}}(E)}{4n_r^2} \quad (1)$$

where r^{sp} is the *internal* spontaneous emission spectrum, $\alpha(E)$ is the absorption spectrum and n_r the refractive index of the medium. $a(E)$ is the spectral absorptivity defined as expression (2) with R the reflection from the outside onto the sample surface, and d the thickness of the conceptual slab [25].

$$a(E) = (1 - R(E))\Big[1 - \exp\left(-\alpha(E)d\right)\Big] \quad (2)$$

Note that d is also considered as a characteristic length scale over which carriers are generated, travel and recombine radiatively [25]. Based on this definition, this parameter should be inversely proportional to the absorption coefficient at the excitation wavelength i.e. $d \approx 1/\alpha(\lambda_{\mathrm{laser}})$. However, the PL spectrum will mostly be centered around the bandgap energy where the $\alpha(E)$ is at least one or two orders of magnitude smaller than $\alpha(\lambda_{\mathrm{laser}})$, in the case of non-resonant excitation. Therefore $\alpha d << 1$ and the absorbance $a(E)$ can be simplified by expanding the exponent with a Taylor series such that $a(E) \approx A\alpha(E)$. In that case, the PL intensity from equation (1) becomes

$$I_{\mathrm{PL}}(E) \approx \frac{2\pi A}{\hbar^3 c^2} \frac{E^2 \alpha(E)}{\exp\left(\frac{E-\Delta\mu}{k_{\mathrm{B}}T}\right) - 1} \approx \frac{A}{4n_r^2} \cdot r^{\mathrm{sp}}(E) \quad (3)$$

With this approximation, The PL spectrum intensity is therefore entirely defined by the internal spontaneous emission spectrum or the absorption spectrum depending on the formula used.

The spontaneous emission spectrum r^{sp} is calculated using the Fermi's golden rule [26, 27] and the perturbation theory as described in equation (4):

$$r^{\mathrm{sp}}(\hbar\omega) = \frac{\hbar\omega\Lambda}{V} \sum_{c,v,\vec{k}} \left| \left\langle \Phi_c(\vec{k}) \middle| \frac{\hbar}{m_0} \hat{\varepsilon}.\vec{p} \middle| \Phi_v(\vec{k}) \right\rangle \right|^2 f\left(\epsilon_c, \mu_e\right) \times \delta\left(\epsilon_c(\vec{k}) - \epsilon_v(\vec{k}) - \hbar\omega\right) \left[1 - f(\epsilon_v, \mu_h)\right], \quad (4)$$

where, $\Lambda = n_r e^2/\pi c^3 \varepsilon_0 \hbar^4$ is a material-related constant with e the elementary charge, n_r the refractive index of the material, and c the speed of light in vacuum. V is the volume of the states in the $\vec{k}$-space. The summations are done over the different values of $\vec{k}$ in the Brillouin zone (BZ) to account for the possible transitions between the conduction and the valence bands. The Dirac delta distribution is used to limit the transitions to those with an energy difference of $\hbar\omega$, the photon energy. Moreover, $M_{i,f}^2(\vec{k}) = \left|\left\langle \Phi_f(\vec{k}) \middle| \frac{\hbar}{m_0} \hat{\varepsilon}.\vec{p} \middle| \Phi_i(\vec{k}) \right\rangle\right|^2$ represents the strength of the transition from the state $|\Phi_i\rangle$ to $|\Phi_f\rangle$ with $\hat{\varepsilon}$ the polarization unit vector and $\vec{p}$ the momentum matrix operator. Finally, the Fermi-Dirac statistic is used to account for the probability occupation of the different states, with f given by $f(\epsilon, \mu) = \left[1 + \exp\left(\frac{\epsilon-\mu}{k_{\mathrm{B}}T}\right)\right]^{-1}$ in which ϵ is the energy and μ the Fermi-level of the charge carrier described by the function.

The computation of the spontaneous emission spectrum requires prior knowledge of the band structure of the semiconductors, the momentum matrix elements, and the quasi-Fermi levels, as seen in equation (4). In the current literature, for a single bulk direct bandgap semiconductor, r^{sp} is commonly computed using the JDOS model [28–30]. This model relies on the parabolic band approximation (PBA) which leads to a set of relatively easy analytical formulas. It is mostly accurate for a non-degenerately doped semiconductor in weak-injection regime with the quasi-Fermi levels lying within the bandgap and away from the different band edges by several $k_{\mathrm{B}}T$, where k_B is the Boltzmann's constant and T the temperature ($\Delta\mu \approx 0$). This model was extended in [31] to account for different excitation regimes by explicitly evaluating the quasi-Fermi level splitting $\Delta\mu$, and the non-equilibrium absorption spectrum in equation (3). However, it still relies on the PBA which restricts the analysis. Indeed, for higher excitation power and/or doping concentration, μ_e and μ_h would shift towards, and even beyond, the band edges where the PBA should be less accurate. Besides, for a biaxially strained semiconductor, the $\vec{k}$ direction degeneracies in the BZ are expected to be broken. In this situation, the band dispersion would be increasingly anisotropic, thus challenging one of the core principles of the PBA. A more accurate theoretical framework is therefore required for the computation of the spontaneous emission spectrum r^{sp}, and the description of the measured PL spectra.

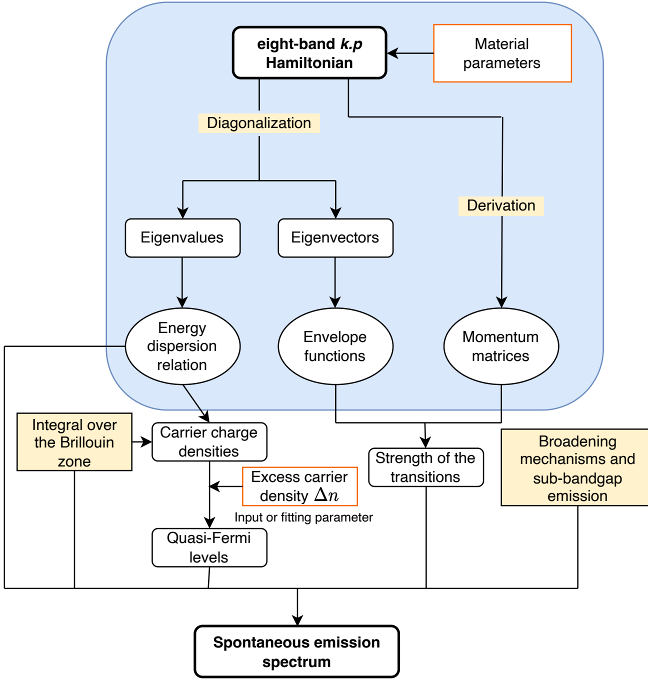

FIG. 1. Different steps followed in the computation of the spontaneous emission spectra

A. Spontaneous emission spectrum and eight-band *k.p* formalism

The spectrum r^{sp} is computed using the eight-band $k.p$ formalism together with the EFA [32], following the simulation workflow summarized in Fig. 1. The eight-band $k.p$ $\mathrm{Ge}_{1-x}\mathrm{Sn}_x$ material parametrization is based on early reports [33–35], while strain implementation is based on the Bir-Pikus formalism [36]. To account for the inaccuracy of the Vegard's law to estimate the bandgaps of $\mathrm{Ge}_{1-x}\mathrm{Sn}_x$ alloys, bandgap bowing parameters are introduced for L and Γ high-symmetry points. Unlike the JDOS model (and all the different models relying on the PBA), the evolution of the strength of the optical transitions with the wave vector $\vec{\boldsymbol{k}}$ is explicitly computed using the formalism developed by Szmulowicz [37]. If $|\Phi_i\rangle$ and $|\Phi_f\rangle$ are the initial and final states within the EFA, the strength of the transition is given by [37]:

$$\left\langle \Phi_i \middle| \frac{\hbar}{m_0}\hat{\mathbf{e}}.\vec{\boldsymbol{p}} \middle| \Phi_f \right\rangle = \sum_{\mu,\,\nu} \Phi^*_{i,\mu}(\vec{\boldsymbol{k}}) \left(\hat{\varepsilon} \cdot \frac{\partial \mathcal{H}_{\mu\nu}(\vec{\boldsymbol{k}})}{\partial \vec{\boldsymbol{k}}} \right) \Phi_{f,\nu}(\vec{\boldsymbol{k}}) = \sum_{\mu,\,\nu,\,l} \Phi^*_{i,\mu}(\vec{\boldsymbol{k}}) \left[\varepsilon_l \cdot \left(\frac{\partial \mathcal{H}_{\mu\nu}}{\partial k_l} \right) \right] \Phi_{f,\nu}(\vec{\boldsymbol{k}}), \tag{5}$$

where $\Phi_{i,\mu}$ and $\Phi_{f,\nu}$ are the coefficients of the envelope function vector related to the states $|\Phi_i\rangle$ and $|\Phi_f\rangle$, respectively. The unit vector $\hat{\varepsilon}$ gives the polarization of the incident light, while $\partial\mathcal{H}_{\mu\nu}(\vec{\boldsymbol{k}})/\partial\vec{\boldsymbol{k}}$ is the derivative of the $k.p$ Hamiltonian with respect to the wave vector $\vec{\boldsymbol{k}}$. The expressions of the different momentum matrices $\partial\mathcal{H}_{\mu\nu}/\partial k_l$ can be found in the Supporting information S1 [38] .

For a given value of the optically injected carrier density Δn, if n_0 and p_0 denote the total electrons and holes' charge densities at thermal equilibrium, the quasi-Fermi levels μ_e (for electrons) and μ_h (for holes) are determined by solving the set of equations (6):

$$\begin{aligned} n_0 + \Delta n &= \frac{1}{(2\pi)^3} \sum_{i\in\mathrm{CB}} \int_{\mathrm{BZ}} \frac{d^3\vec{\boldsymbol{k}}}{1+\exp\left(\frac{\epsilon_i(\vec{\boldsymbol{k}})-\mu_e}{kT}\right)} \\ p_0 + \Delta n &= \frac{1}{(2\pi)^3} \sum_{i\in\mathrm{VB}} \int_{\mathrm{BZ}} \frac{d^3\vec{\boldsymbol{k}}}{1+\exp\left(\frac{\mu_h-\epsilon_j(\vec{\boldsymbol{k}})}{kT}\right)} \end{aligned} \tag{6}$$

Herein, the conduction band electrons are assumed to be shared between the Γ and L valleys. This assumption is only relevant when the energy band offset between these valleys is relatively close to the thermal energy $k_{\mathrm{B}}T$ to enable the electrons to transition between them. The carrier concentration n_0 and p_0 are evaluated after solving the electroneutrality equation to estimate the thermal equilibrium Fermi level E_f. Besides, the computation of the integrals over the BZ, required for estimating the quasi-Fermi levels and r^{sp}, relies on the special-lines approximation (SLA) [39]. Within this approximation, the three-dimensional BZ integrals are replaced by a sum of one-dimensional integrals over some characteristic directions (denoted as "special") of the crystal lattice. These directions could, for example, be the symmetry directions used in the eight-band $k.p$ formalism. If we denote by $\mathcal{L}$ the set of the special directions, the electrons density from equation (6) becomes

$$n = \frac{1}{2\pi^2} \sum_{\substack{D\in\mathcal{L}\\ i\in\mathrm{CB}}} w_D \left(\int_0^{k_{\mathrm{BZ}}} \frac{k_D^2 \mathrm{d}k_D}{1+\exp\left(\frac{\epsilon_i(k_D)-\mu_e}{kT}\right)} \right) \tag{7}$$

with w_D the weight of the direction D, $\epsilon_i(k_{\mathrm{D}})$ the energy of the conduction band i at k_{D} and $k_{\mathrm{BZ}} \sim 0.5$ (units of π/a_0, a_0 being the lattice constant of the material) for the eight-band $k.p$ model to still be accurate. Depending on the computation, the exact value of the upper limit k_{BZ} could be neglected since the integrands are expected to vanish rapidly while increasing the value of k_{D}. More information about all the different directions considered in our framework can be found in the Supporting information S2 [38]. Unlike the PBA, which leads to parabolic and isotropic-like band structure, this method accounts for the anisotropy and the non-parabolicity of the bands obtained with the $k.p$ theory and approximates the warping of real bands. It is, therefore, expected to be more accurate.

The theoretical spontaneous emission spectrum developed previously is often insufficient to accurately describe the PL spectrum. Indeed, the sub-bandgap emission resulting from carrier disorders and broadening mecha-

nisms in the materials is not accounted for in equation (4) [40–42]. To include these contributions, the theoretical spectrum r^{sp}_{ideal} from equation (4) is convoluted with a broadening function $\mathcal{B}$, as outlined in equation (8).

$$r^{sp}(\hbar\omega) = \int_{-\infty}^{+\infty} r^{sp}_{ideal}(\epsilon) \cdot \mathcal{B}(\hbar\omega - \epsilon) d\epsilon \quad (8)$$

The broadening function $\mathcal{B}$ is usually chosen as a Gaussian or a Lorentzian to account for the inhomogeneous and homogeneous broadening mechanisms, respectively. However, the Lorentzian function was reported to sometimes overestimate the effects of the homogeneous broadening due to its slowly decaying tails. For that reason, it is usually replaced by a hyperbolic secant function [43].

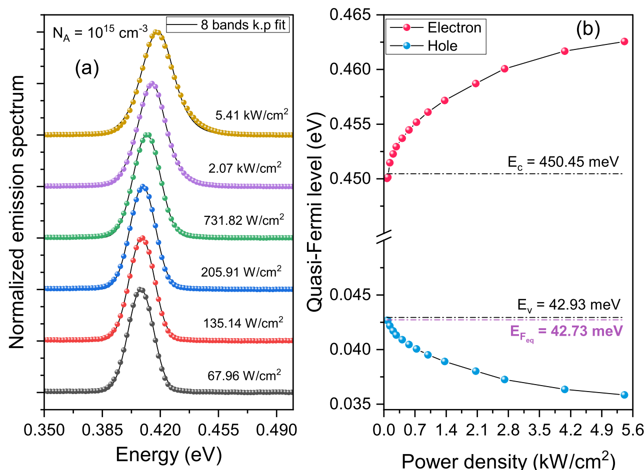

FIG. 2. (a) Power-dependent photoluminescence at 4 K for the -1.27% biaxially strained $Ge_{0.83}Sn_{0.17}$. The scatter points are from the measurements while the black lines are the results from the simulations. (b) Evolution of the extracted quasi-Fermi levels (μ_e, μ_h) with the power density.

B. Spontaneous emission intensity and steady-state radiative carrier lifetime

We shall use the symbol $R^{\hat{\varepsilon}}_{sp}$ to denote the rate of polarization-dependent spontaneous emission per unit volume, where $\hat{\varepsilon}$ gives the polarization of the incident light. The quantity $R^{\hat{\mathbf{e}}}_{sp}$ is generally defined as the integral of the polarization-dependent spontaneous emission spectrum over the range of photon energy bigger than the band-gap of the material, and given by equation (9) [26].

$$R^{\hat{\varepsilon}}_{sp} = \int_{0}^{+\infty} r^{sp}_{\hat{\varepsilon}}(\hbar\omega)\, d\hbar\omega \quad (9)$$

For an unpolarized incident light, the total spontaneous emission rate per unit volume R_{sp} is defined as the average of the contributions from the three polarizations defined by the unit vectors $\hat{\varepsilon}_x = (1, 0, 0)$, $\hat{\varepsilon}_y$ and $\hat{\varepsilon}_z$.

The steady-state radiative carrier lifetime τ_{rad} is determined by the net rate of spontaneous emission R^{net}_{sp} and the density of photo-excited carriers Δn (equation (10)). R^{net}_{sp} is defined as the amount by which the non-equilibrium spontaneous recombination rate R_{sp} exceeds the thermal equilibrium generation rate G_0, which is the same as the thermal equilibrium spontaneous emission rate.

$$\tau_{rad} = \frac{\Delta n}{R^{net}_{sp}} \quad (10)$$

R^{net}_{sp} is usually estimated using equation (11), in which B is a material-dependent parameter known as the bimolecular recombination coefficient. In that case, τ_{rad} becomes relatively easy to compute, as presented in equation (12).

$$R^{net}_{sp} = R^{neq}_{sp} - R^{eq}_{sp} = B(np - n_0 p_0) \quad (11)$$

$$\tau_{rad} = \frac{1}{B(\Delta n + n_0 + p_0)} \quad (12)$$

The bimolecular recombination coefficient B is typically assumed to be independent of Δn (and, therefore, the quasi-Fermi levels). However, this approximation is not always accurate. For example, B was previously shown to vary linearly with the excess carrier density Δn in III-V semiconductors [44–46]. For that reason, it is reasonable to rely only on equations (9) and (10), which state the general case without any specific approximations.

III. RESULTS AND DISCUSSION

The accuracy of the established theoretical framework has been evaluated through the analysis of the PL spectra recorded as a function of the excitation power and temperature from $Ge_{0.83}Sn_{0.17}$ layers [47]. The epitaxial growth of these layers was achieved using low-pressure chemical vapor deposition (LP-CVD) starting from a 600 - 700 nm Ge virtual substrate on a 4 inch Si wafer. To ensure the growth of a $Ge_{0.83}Sn_{0.17}$ layer with a uniform Sn composition, a multilayer heterostructure consisting of top layer (TL)/middle layer (ML)/bottom layer (BL) was grown while the incorporation of Sn in each layer is controlled by adjusting the growth temperature. More details on the growth and characterization of $Ge_{0.83}Sn_{0.17}$ material can be found in [47].

In as-grown $Ge_{0.83}Sn_{0.17}$ layers, the band alignment favors the electrons and holes diffusion to the TL, where they should recombine. Indeed, the PL spectra are confirmed to originate from carrier recombination in this specific layer [47]. Therefore, from a theoretical standpoint, it would be judicious to analyze the PL results as if they were emitted by a bulk GeSn material with a 17 at. % Sn composition. On this basis, the different power-dependent PL spectra, recorded at 4 K, were simulated by iteratively evaluating r^{sp} as well as the excess

carrier concentration Δn and γ the full width at half maximum (FWHM) of the broadening function. To solve equations (6), and extract the quasi-Fermi levels couple (μ_e, μ_h), the p-type background doping was considered to be around $10^{15}\,\mathrm{cm}^{-3}$ at 4 K. This value was chosen with reference to the p-type background doping estimated between 1×10^{17} and $5\times10^{17}\,\mathrm{cm}^{-3}$ at 300 K [48].

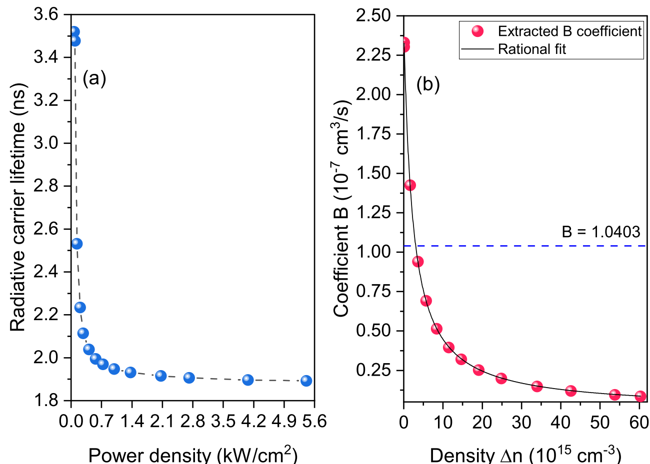

FIG. 3. (a) Evolution of the radiative carrier lifetime as a function of the excitation power density P_{exc}, (b) Evolution of the B coefficient as a function of the excess carrier density Δn. The solid spheres represent the values of B computed from the extracted Δn, R_{sp} using equation (11), while the black line is the result of a fit using a rational function.

Fig. 2(a) displays the measured and simulated spectra for the as-grown $\mathrm{Ge_{0.83}Sn_{0.17}}$ material. For each power density, a coefficient of determination (R^2) of around 99.5% is obtained, thus highlighting the accuracy of the simulated spectra. Moreover, the evolution of the extracted quasi-Fermi levels with the excitation power density P_{exc} is outlined in Fig. 2(b). For a p-type background doping of $10^{15}\,\mathrm{cm}^{-3}$, the thermal equilibrium Fermi level E_{F} is about 42.73 meV. As shown in Fig. 2(b), the non-degenerate semiconductor approximation is not appropriate here since E_{F} is less than the top valence band edge located around 42.93 meV. Starting from a power density of 67.95 W/cm^2, both the electrons and holes quasi-Fermi levels start to deviate from E_{F}. In fact, a progressive increase from 450.02 to 462.57 meV is observed for the quasi-Fermi level μ_e, causing the electron concentration to increase. Simultaneously, the holes quasi-Fermi level μ_h decreases while remaining very close to the thermal equilibrium level with a maximum offset of 6.88 meV at 5.4 kW/cm^2. While these variations may be perceived as small, they are not insignificant. Indeed, with the thermal energy of about 0.34 meV at 4 K, one should expect a noticeable increase in the spontaneous emission intensity R_{sp}. Moreover, using equation (10), the steady-state radiative carrier lifetime τ_{rad} was extracted (Fig. 3(a)) and shown to decrease from 3.52 to 1.89 ns in the range of power density used in this study.

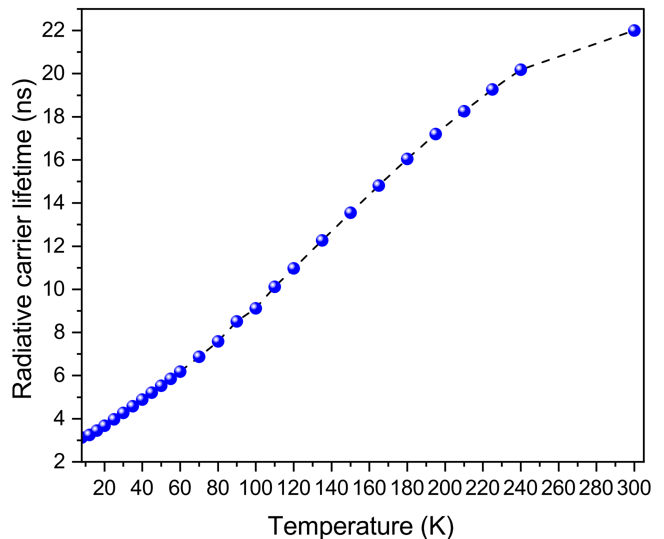

FIG. 4. Evolution of the radiative carrier lifetime as function of temperature for the as-grown $\mathrm{Ge_{0.83}Sn_{0.17}}$.

Besides, the accuracy of equation (11) was also evaluated using the different parameters obtained from the analysis above. Indeed, the bimolecular recombination coefficient B was computed from the extracted values of R_{sp} and Δn and its behavior is outlined in Fig. 3(b). Rather than being constant, it decreases with Δn, as suggested earlier for III-V semiconductors [44, 45]. However, its evolution for the as-grown $\mathrm{Ge_{0.83}Sn_{0.17}}$ is not as linear as presented by Olshansky et al. for InGaAsP and AlGaAs light sources [46]. In fact, after performing a fit of the obtained data, B was shown to evolve with Δn following a rational function (Fig. 3(b)). Additionally, for Δn above $10^{15}\,\mathrm{cm}^{-3}$, the values extracted were shown to be lower than the value of $1.04\times10^{-7}\,\mathrm{cm}^3/\mathrm{s}$ computed assuming parabolic band dispersion and the non-degenerate semiconductor approximation.

The impact of temperature on the steady-state radiative carrier lifetime has also been investigated. Herein, assuming a p-type background doping of $1\times10^{15}\,\mathrm{cm}^{-3}$ at 4 K and $1\times10^{17}\,\mathrm{cm}^{-3}$ at 300 K, which is in line with recent measurements [48], the evolution of the doping with temperature was estimated. Using these values, the temperature-dependent PL spectra were simulated with the theoretical estimation of the spontaneous emission spectrum from the framework described above, and the evolution of τ_{rad} was extracted for the as-grown $\mathrm{Ge_{0.83}Sn_{0.17}}$, as displayed in Fig. 4. Note that from this analysis, a minimum R^2 factor of about 98% was observed throughout the 4-300 K range. The estimated steady-state radiative carrier lifetime τ_{rad} increases with the temperature from $\sim$ 3.2 ns at 10 K to $\sim$ 22.2 ns at 300 K. These values are very comparable to the reported recombination lifetimes in literature for III-V compound semiconductors, which are generally in the nanoseconds range [49–51]. They are also of the same order of magnitude as the values for Ge calculated from first principles

[52]. Indeed, the radiative lifetime for Ge in the diamond structure was shown to be around 10 ns for T below 300 K.

Finally, to appreciate the radiative emission strength of $Ge_{1-x}Sn_x$ with respect to other direct bandgap semiconductors, we compare the radiative emission rate or more precisely the bimolecular recombination coefficient B. Using the same process as for the power-dependent PL, B is extracted as a function of the temperature. From this analysis, B is found to evolve following the allometric power law aT^b with $b \approx -1.5143$, and reaching $3.81 \times 10^{-10}\,\mathrm{cm^3/s}$ at 240 K. This value is comparable to those extracted at 300 K for GaAs ($3.5 \times 10^{-10}\,\mathrm{cm^3/s}$), InP ($1.2 \times 10^{-10}\,\mathrm{cm^3/s}$), and hexagonal $Si_{0.20}Ge_{0.80}$ ($0.7 \times 10^{-10} - 11 \times 10^{-10}\,\mathrm{cm^3/s}$).

IV. CONCLUSION

To circumvent the limitations in the experimental studies of carrier dynamics in narrow bandgap $Ge_{1-x}Sn_x$ materials, this work demonstrates a straightforward method to obtain the carrier radiative lifetime from simple PL spectra. The approach relies on a theoretical framework combining the band structure calculations using the $k.p$ formalism together with the envelope function approximation to estimate the absorption and spontaneous emission spectra. This framework simulates accurately the experimental measurements thereby allowing the evaluation of the steady-state radiative carrier lifetime from the net rate of spontaneous emission and the density of photo-excited carriers. For a $Ge_{0.83}Sn_{0.17}$ material under an in-plane biaxial compressive strain $\varepsilon_{\parallel} = -1.3\%$, the analysis revealed a lifetime τ_{rad} in the nanoseconds range increasing from 3 to 22 ns for temperatures between 10 and 300 K. Additionally, the introduced model also solves the restrictions that are inherent to the joint density of states (JDOS) model resulting from the parabolic band approximation (PBA) and the weak-injection approximation.

ACKNOWLEDGEMENTS

O.M. acknowledges support from NSERC Canada (Discovery, SPG, and CRD Grants), Canada Research Chairs, Canada Foundation for Innovation, Mitacs, PRIMA Québec, Defence Canada (Innovation for Defence Excellence and Security, IDEaS), the European Union's Horizon Europe research and innovation programme under grant agreement No 101070700 (MIRAQLS), and the US Army Research Office Grant No. W911NF-22-1-0277.

AUTHORS INFORMATION

Corresponding Author:
† oussama.moutanabbir@polymtl.ca

Notes:
The authors declare no competing financial interest.

[1] O. Moutanabbir, S. Assali, X. Gong, E. O'Reilly, C. A. Broderick, B. Marzban, J. Witzens, W. Du, S.-Q. Yu, A. Chelnokov, D. Buca, and D. Nam, Applied Physics Letters **118**, 110502 (2021).

[2] M. R. M. Atalla, S. Assali, A. Attiaoui, C. Lemieux-Leduc, A. Kumar, S. Abdi, and O. Moutanabbir, Advanced Functional Materials **31**, 2006329 (2021).

[3] M. R. M. Atalla, S. Assali, S. Koelling, A. Attiaoui, and O. Moutanabbir, ACS Photonics **9**, 1425 (2022).

[4] D. Buca, A. Bjelajac, D. Spirito, O. Concepción, M. Gromovyi, E. Sakat, X. Lafosse, L. Ferlazzo, N. von den Driesch, Z. Ikonic, D. Grützmacher, G. Capellini, and M. El Kurdi, Advanced Optical Materials **10**, 2201024 (2022).

[5] C.-Y. Chang, P.-L. Yeh, Y.-T. Jheng, L.-Y. Hsu, K.-C. Lee, H. Li, H. H. Cheng, and G.-E. Chang, Photonics Research **10**, 2278 (2022).

[6] J. Chrétien, N. Pauc, F. Armand Pilon, M. Bertrand, Q.-M. Thai, L. Casiez, N. Bernier, H. Dansas, P. Gergaud, E. Delamadeleine, R. Khazaka, H. Sigg, J. Faist, A. Chelnokov, V. Reboud, J.-M. Hartmann, and V. Calvo, ACS Photonics **6**, 2462 (2019).

[7] J. Chrétien, Q. M. Thai, M. Frauenrath, L. Casiez, A. Chelnokov, V. Reboud, J. M. Hartmann, M. El Kurdi, N. Pauc, and V. Calvo, Applied Physics Letters **120**, 051107 (2022).

[8] A. Elbaz, D. Buca, N. von den Driesch, K. Pantzas, G. Patriarche, N. Zerounian, E. Herth, X. Checoury, S. Sauvage, I. Sagnes, A. Foti, R. Ossikovski, J.-M. Hartmann, F. Boeuf, Z. Ikonic, P. Boucaud, D. Grützmacher, and M. El Kurdi, Nature Photonics **14**, 375 (2020).

[9] H.-J. Joo, Y. Kim, D. Burt, Y. Jung, L. Zhang, M. Chen, S. J. Parluhutan, D.-H. Kang, C. Lee, S. Assali, Z. Ikonic, O. Moutanabbir, Y.-H. Cho, C. S. Tan, and D. Nam, Applied Physics Letters **119**, 201101 (2021).

[10] Y. Jung, D. Burt, L. Zhang, Y. Kim, H.-J. Joo, M. Chen, S. Assali, O. Moutanabbir, C. S. Tan, and D. Nam, Photonics Research **10**, 1332 (2022).

[11] X. Li, L. Peng, Z. Liu, Z. Zhou, J. Zheng, C. Xue, Y. Zuo, B. Chen, and B. Cheng, Photonics Research **9**, 494 (2021).

[12] X. Liu, J. Zheng, C. Niu, T. Liu, Q. Huang, M. Li, D. Zhang, Y. Pang, Z. Liu, Y. Zuo, and B. Cheng, Photonics Research **10**, 1567 (2022).

[13] L. Luo, S. Assali, M. R. M. Atalla, S. Koelling, A. Attiaoui, G. Daligou, S. Martí, J. Arbiol, and O. Moutanabbir, ACS Photonics **9**, 914 (2022).

[14] B. Marzban, L. Seidel, T. Liu, K. Wu, V. Kiyek, M. H. Zoellner, Z. Ikonic, J. Schulze, D. Grützmacher, G. Capellini, M. Oehme, J. Witzens, and D. Buca, ACS Photonics , acsphotonics.2c01508 (2022).

[15] E. Talamas Simola, V. Kiyek, A. Ballabio, V. Schlykow, J. Frigerio, C. Zucchetti, A. De Iacovo, L. Colace, Y. Yamamoto, G. Capellini, D. Grützmacher, D. Buca, and G. Isella, ACS Photonics **8**, 2166 (2021).

[16] H. Tran, T. Pham, J. Margetis, Y. Zhou, W. Dou, P. C. Grant, J. M. Grant, S. Al-Kabi, G. Sun, R. A. Soref, J. Tolle, Y.-H. Zhang, W. Du, B. Li, M. Mortazavi, and S.-Q. Yu, ACS Photonics **6**, 2807 (2019).

[17] S. Xu, W. Wang, Y.-C. Huang, Y. Dong, S. Masudy-Panah, H. Wang, X. Gong, and Y.-C. Yeo, Optics Express

27, 5798 (2019).
[18] Y. Zhou, Y. Miao, S. Ojo, H. Tran, G. Abernathy, J. M. Grant, S. Amoah, G. Salamo, W. Du, J. Liu, J. Margetis, J. Tolle, Y.-h. Zhang, G. Sun, R. A. Soref, B. Li, and S.-Q. Yu, Optica **7**, 924 (2020).
[19] B. Julsgaard, N. von den Driesch, P. Tidemand-Lichtenberg, C. Pedersen, Z. Ikonic, and D. Buca, Photon. Res. **8**, 788 (2020).
[20] E. Vitiello, S. Rossi, C. A. Broderick, G. Gravina, A. Balocchi, X. Marie, E. P. O'Reilly, M. Myronov, and F. Pezzoli, Phys. Rev. Applied **14**, 064068 (2020).
[21] M. K. Hudait, S. W. Johnston, M. B. Clavel, S. Bhattacharya, S. Karthikeyan, and R. Joshi, Journal of Materials Chemistry C **10**, 10530 (2022).
[22] B. E. A. Saleh, *Fundamentals of Photonics*, Wiley Series in Pure and Applied Optics (Wiley, 2019).
[23] G. Lasher and F. Stern, Phys. Rev. **133**, A553 (1964).
[24] P. Wurfel, Journal of Physics C: Solid State Physics **15**, 3967 (1982).
[25] J. K. Katahara and H. W. Hillhouse, Journal of Applied Physics **116**, 173504 (2014).
[26] S. L. Chuang, *Physics of Photonic Devices*, 2nd ed., Wiley Series in Pure and Applied Optics (Wiley, 2009).
[27] P. T. Landsberg, *Recombination in Semiconductors*, 1st ed. (Cambridge University Press, 1992).
[28] E. F. Schubert, *Light-Emitting Diodes*, 2nd ed. (Cambridge University Press, 2006).
[29] D. Stange, *Group IV (Si)GeSn light emission and lasing studies*, Dissertation, RWTH Aachen University, Jülich (2019), druckausgabe: 2019. - Onlineausgabe: 2019. - Auch veröffentlicht auf dem Publikationsserver der RWTH Aachen University; Dissertation, RWTH Aachen University, 2019.
[30] S. Wirths, *Group IV epitaxy for advanced nano- and optoelectronic applications*, Dissertation, RWTH Aachen, Jülich (2016), druckausgabe: 2016. - Onlineausgabe: 2016. - Auch veröffentlicht auf dem Publikationsserver der RWTH Aachen University; Dissertation, RWTH Aachen, 2015.
[31] A. Dijkstra, *Optical properties of direct band gap group IV semiconductors*, Ph.D. thesis, Applied Physics and Science Education (2021), proefschrift. - Embargo 1 year, pdf open access 28-5-2022.
[32] T. B. Bahder, Physical Review B **41**, 11992 (1990).
[33] G.-E. Chang, S.-W. Chang, and S. L. Chuang, IEEE Journal of Quantum Electronics **46**, 1813 (2010).
[34] K. Lu Low, Y. Yang, G. Han, W. Fan, and Y.-C. Yeo, Journal of Applied Physics **112**, 103715 (2012).
[35] M. P. Polak, P. Scharoch, and R. Kudrawiec, Journal of Physics D: Applied Physics **50**, 195103 (2017).
[36] G. L. Bir and G. E. Pikus, *Symmetry and strain-induced effects in semiconductors* (Wiley, 1974).
[37] F. Szmulowicz, Physical Review B **51**, 1613 (1995).
[38] See Supplemental Material for more details about the momentum matrix elements and the special points approximation.
[39] P. Enders, Semiconductor Science and Technology **11**, 187 (1996).
[40] E. F. Schubert, E. O. Göbel, Y. Horikoshi, K. Ploog, and H. J. Queisser, Physical Review B **30**, 813 (1984).
[41] D. Ouadjaout and Y. Marfaing, Physical Review B **41**, 12096 (1990).
[42] M. Asada, IEEE Journal of Quantum Electronics **25**, 2019 (1989).
[43] W. W. Chow, S. W. Koch, and M. Sargent, Semiconductor-laser physics (Springer-Verlag, Berlin ; New York, 1997) pp. 94–95.
[44] F. Stern, Journal of Applied Physics **47**, 5382 (1976).
[45] C. B. Su, R. Olshansky, J. Manning, and W. Powazinik, Applied Physics Letters **44**, 732 (1984).
[46] R. Olshansky, C. Su, J. Manning, and W. Powazinik, IEEE Journal of Quantum Electronics **20**, 838 (1984).
[47] S. Assali, A. Dijkstra, A. Attiaoui, E. Bouthillier, J. Haverkort, and O. Moutanabbir, Physical Review Applied **15**, 024031 (2021).
[48] M. R. M. Atalla, S. Assali, A. Attiaoui, C. Lemieux-Leduc, A. Kumar, S. Abdi, and O. Moutanabbir, Advanced Functional Materials **31**, 2006329 (2021).
[49] J. Feldmann, G. Peter, E. O. Göbel, P. Dawson, K. Moore, C. Foxon, and R. J. Elliott, Phys. Rev. Lett. **59**, 2337 (1987).
[50] J. Bellessa, V. Voliotis, R. Grousson, X. L. Wang, M. Ogura, and H. Matsuhata, Phys. Rev. B **58**, 9933 (1998).
[51] G. 't Hooft, M. Leys, and H. Talen-v.d. Mheen, Superlattices and Microstructures **1**, 307 (1985).
[52] C. Rödl, J. Furthmüller, J. R. Suckert, V. Armuzza, F. Bechstedt, and S. Botti, Phys. Rev. Mater. **3**, 034602 (2019).